ON PERFORMANCE OF HIGH-EFFICIENCY FERRITE MEANDER ANTENNA (HEMA) FOR MIMO COMMUNICATIONS

Chandana K. K. Jayasooriya[1, *], Hyuck M. Kwon[1] Ryan Syslo[2], Yang-Ki Hong[2], Jaejin Lee[2], and Gavin Abo[2]

[1]Department of Electrical Engineering and Computer Science, Wichita State University, 1845 Fairmount, Wichita, KS 67260, USA

[2]Department of Electrical and Computer Engineering, The University of Alabama, Tuscaloosa, AL 35487, USA

Abstract—This paper presents a high-efficiency ferrite meander antenna (HEMA), which can be used to realize a 2×2 multiple-input-multiple-output (MIMO) communication system when it is used at both the transmitter and the receiver ends. This antenna is designed to operate at 2.45 GHz center frequency (f_c). It consists of two spatially separated half-cycle microstrip meander structures. Ferrite material is not used for the entire substrate, only beneath each meander structure. A standard FR-4 substrate is utilized as a system board. Impedance bandwidth and radiation patterns of the fabricated antenna are measured and compared with those of the simulation results. The $-10\,\mathrm{dB}$ impedance bandwidth of the fabricated antenna is 262 MHz, whereas the simulated bandwidth is 235 MHz. According to the simulations, the gain and efficiency of the antenna are 2.2 dB and 81%, respectively. The efficiency of the antenna is confirmed by measurements. By using the simulated radiation patterns, correlation between the radiation patterns is calculated and employed in the generation of the channel matrix. Mutual impedance of the antennas and antenna efficiency are also included in the channel matrix, which in turn is used in bit error rate (BER) and ergodic capacity simulations. BER and ergodic capacity are utilized as performance metrics. The effect of antenna efficiency, mutual impedance of the antennas, and correlation between radiation patterns on system performance are presented.

1. INTRODUCTION

It is well known that if multiple antennas are used at both the transmitter and the receiver, then the maximum number of bits correctly delivered per unit time and unit bandwidth, i.e., capacity, can be significantly increased. The capacity of a multiple-input (transmit)-multiple-output (receive) (MIMO) system can be much higher than that of a single-input-single-output (SISO) system [1] and increases linearly with the number of antennas in the presence of a rich scattering environment, which ensures that the signal from each transmit antenna becomes uncorrelated. According to Shannon's classical formula in the high signal-to-noise ratio (SNR) realm, the capacity of a SISO system increases one bit/(s·Hz) for every 3 dB increase in SNR. Hence, in a MIMO system with n antennas at both the transmitter and the receiver, for the case of independent Rayleigh faded paths among TX and RX antenna elements, capacity increases with n bits/(s·Hz) for every 3 dB of SNR improvement [2].

As it suggests, the capacity of a MIMO system can be significantly increased by adding more antenna elements. Decreasing the space between antennas in order to place more antennas in a designated area results in two negative effects. One is the increasing correlation among transmitted signals, and the second is the increasing mutual coupling among antennas [2]. Mutual coupling is a function of antenna spacing, number of antennas, and direction of each ray relative to the array plane. Hence, it becomes difficult to match the antenna impedance, which is important for efficient energy transfer [2]. Making the antenna spacing lower than $\lambda/2$ would cause performance degradation due to the aforementioned effects, where $\lambda = c/f_c$ denotes the wavelength in meters for carrier frequency f_c (Hz) and the speed of light c (m/s). For example, when $f_c = 2.45$ GHz, the minimum required adjacent antenna spacing of $\lambda/2$ would be 6 cm, which can be prohibitive in many space-limited applications, such as handsets, because the number of antennae increases.

Different diversity techniques, e.g., spatial, polarization, and pattern diversity, have been proposed to reduce correlation among subchannels in a MIMO communication system. Up to six degrees of freedom are available in polarization diversity in a rich scattering environment, which can increase the channel capacity significantly [3]. However, the effective degrees of freedom are reduced to three in a real environment, because the channels are not completely uncorrelated in a polarization diversity scheme [3]. In the implementation, three electric dipoles and three magnetic dipoles were placed orthogonally along the x, y, and z axes. A transceiver array with appropriate dissimilarity in

radiation patterns was introduced in [4] to reduce correlation among subchannels. It was shown that pattern diversity in conjunction with spatial diversity can achieve better channel performance.

Microstrip antennas have been studied in numerous research studies, almost all of which deal with the fundamental mode and a single-feed probe (or port). A two-port higher-order microstrip antenna was studied in [5, 6]. Using several feed probes, higher-order modes were excited in a biconical antenna in [7]. More recently, a circular patch antenna (CPA)-based pattern diversity was introduced and analyzed in [8]. Two colocated, stacked circular patch antennas were used to generate two orthogonal far-field radiation patterns, which in turn showed that a diversity gain can be achieved by exploiting pattern diversity instead of space diversity [8]. Feasibility was demonstrated through simulations showing that a MIMO communication system can be realized using the pattern diversity technique, even where strict size limitations apply. The authors in [9] extended their own work in [8] through simulations, where each of two stacked CPAs (2-CPA) had a single-probe feed. These two feed probes were separated over the azimuth plane so that the generated far-field radiation patterns were approximately orthogonal. A similar configuration, a stacked two-ring patch antenna (2-RPA), was presented in [10]. Here, a ferrite substrate was used to reduce the size of the antenna. A reconfigurable multiport CPA (RCPA) was introduced in [11, 12]. RCPA was also designed to generate two orthogonal radiation patterns. Instead of using two stacked CPAs, a single CPA with two ports was used to excite TM_{13} (mode 3) or TM_{14} (mode 4), by varying the radius of the radiator, which was achieved by using PIN-diodes. A miniaturized single CPA (Ferrite 1-CPA) and a single annular ring antenna (ARA) (Ferrite 1-ARA) with two feed probes were studied in [13–15]. A compact dual-mode (TM_{01} and TM_{11}) microstrip patch antenna was also introduced in [16].

Even though 2-CPA, RCPA, Ferrite 1-CPA, Ferrite 1-ARA, and Ferrite 2-RPA can be used to realize a 2×2 MIMO communication system, they cannot be employed in a mobile handset, such as the current smart phone, due to their size. Since higher-order modes must be excited in these antennas to achieve orthogonal radiation patterns, for a given frequency of operation (f_c) and mode number, the radius of the antenna is fixed [17]. In this case, the radius of the antenna can only be reduced by increasing the permeability and permittivity of the substrate material, which was studied in [13–15]. The drawback is the associated higher losses of ferrite materials, which significantly deteriorate antenna efficiency. Furthermore, they cannot

be used in future commercial cellular communication standards, due to their narrow band of operation. Therefore, this paper focuses on designing spatially separated antennas with dissimilar radiation patterns to exploit the pattern diversity.

Current wireless connectivity standards like 802.11n as well as cellular communication standards, LTE (long-term evolution) and LTE-Advanced standards, employ MIMO technology to achieve higher data rates. A maximum downlink (DL) data rate of 172.8 Mbps and 1 Gbps is supported for a 4×4 single-user MIMO system in LTE and LTE-Advanced standards, respectively. To achieve these high data rates, a signal bandwidth as wide as 200 MHz is required for both uplink (UL) and downlink transmission streams. Therefore, MIMO-capable antennas with wider bandwidth are in high demand.

The authors of [18–26] have proposed MIMO-capable antennas for LTE/LTE-Advanced cellular communication system handsets. Table 1 lists a summary of key parameters of 2×2 MIMO antennas designed to operate in the frequency "Band 41," which spans from 2,496 to 2,690 MHz. The antennas presented in [23–26] are designed to operate in "Band 17," which occupies 704 to 716 MHz (UL) and 734 to 746 MHz (DL), and hence are not listed in Table 1. Even though the dimensions of the printed circuit board (PCB) of the antenna presented in this paper are similar to those listed in Table 1 (except the antenna in [19]), the dimensions of a single antenna element is much smaller. The envelope correlation coefficient, as shown in [27], was calculated and presented in most of the cases. As indicated in Table 1, none of the listed references have considered the evaluation of bit error rate (BER) or capacity of the communication system. Furthermore, the bandwidth is evaluated at a voltage standing wave ratio (VSWR) $< 3 : 1$, which is -6 dB.

In this paper, we propose a half-cycle microstrip high-efficiency meander antenna (HEMA), which can be used to realize a 2×2 MIMO system and analyze its microwave theoretic as well as communication theoretic performance metrics such as S-parameters, antenna efficiency, radiation patterns, BER, and ergodic capacity. The correlation between the antenna radiation patterns are considered, and mutual coupling and radiation efficiency are accounted in for the channel matrix, which was used in BER and capacity calculations. The effect of radiation efficiency on those metrics is presented and compared. The author believes that this paper is the first one to include all of these practical parameters together in the evaluation of an antenna.

2. HEMA ANTENNA DESIGN

The objective is to design an antenna that can be used for 2×2 MIMO applications and with dimensions that fit in a current smart phone. The antenna is modeled in the FEKO electromagnetic simulator to replicate antenna characteristics. The design goals are more than 200 MHz of impedance bandwidth centered at 2.45 GHz, high isolation between antennas (< -20 dB), and high efficiency. Impedance bandwidth is evaluated at VSWR $< 2:1$, which is -10 dB ($|S_{11}|$ and $|S_{22}|$), a more strict condition than that of other antennas listed in Table 1.

Table 1. Comparison of compact MIMO antennas for LTE/LTE-advanced standards.

Antenna	Frequency Band	Bandwidth (MHz)	Eff. (%)	PCB Size (mm²)	Elem. Size (mm²)	Corr. Coeff.
[18]	multiband incl. LTE2500	410 (VSWR $< 3:1$)	-	125×100	33×11	< 0.001
[19]	LTE 2500	280 (VSWR$<2.5:1$)	-	10×20		< 0.25
[20]	LTE 700 & LTE 2500	200 (VSWR $< 3:1$)	97.2	120×50	36×15	
[21]	LTE 2500	790 (VSWR$< 3:1$)	75	90×50	19×10	< 0.008
[22]	multiband incl. LTE 2500	250 (VSWR$< 3:1$)	-	100×50	7×50	0.01
Proposed antenna	LTE 2500	262 (VSWR $< 2:1$)	81	90×60	6×8	< 0.001

The signal received at each antenna must be independent to obtain the benefits of MIMO communication systems. To achieve this, the antennas should be designed so that mutual coupling between antennas becomes minimal. Mutual coupling, which is undesired in MIMO applications, is a function of the spatial separation between antenna elements. Furthermore, high isolation is required between the ports to achieve higher radiation efficiency.

The model of the antenna used in FEKO electromagnetic simulator is shown in Figure 1. The antenna model consists of two spatially separated half-cycle microstrip meander structures. Each of these meander structures is placed on a $8 \times 6 \times 1.5$ mm³ piece of ferrite material. Dimensions of the system board and the
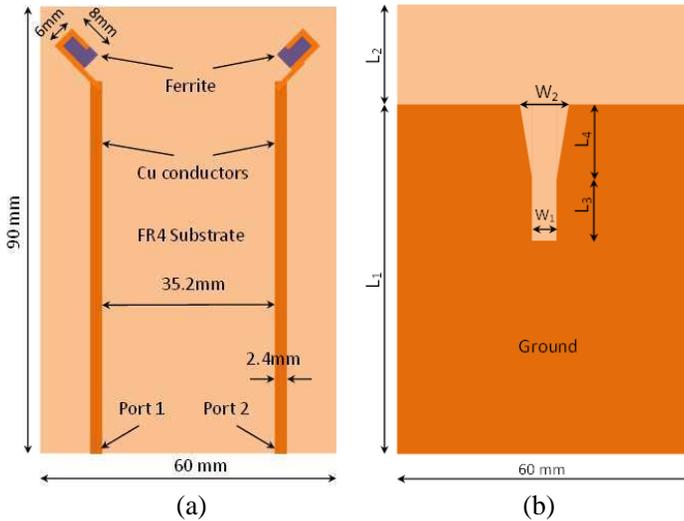
Figure 1. Geometry and dimensions of antenna model. (a) Top view. (b) Bottom view.

antenna configuration are shown in Figure 1(a). Microsrip structures, and ferrite material are shown in orange and purple, respectively. Figure 1(b) shows the bottom view of the antenna. In the proceeding section the values of L_1, W_1, and W_2 are varied to obtain targeted results. The values of L_3 and L_4 are 10 mm and 15 mm, respectively, and are kept constant. The dimensions of the system board ($90 \times 60\,\mathrm{mm}^2$) are not changed ($L_1 + L_2 = 90\,\mathrm{mm}$).

2.1. Ground Plane and Y-Shaped Slit

Initially, S-parameters are simulated simply by varying the length of the ground plane, L_1 (see Figure 1(b)). In this case, the ground plane does not include the Y-shaped slit. The length of the ground plane, L_1, is varied from 90 mm to 60 mm in 5 mm steps. When $L_1 = 90\,\mathrm{mm}$, the backside of the FR4 substrate is entirely covered by the ground plane. Resulting S-parameters are shown in Figure 2. For the sake of clarity, S-parameters related to Port 1 and Port 2 are separated and shown in Figures 2(a) and 2(b), respectively.

As can be seen, $|S_{21}|$ and $|S_{12}|$ are almost identical. Even though S_{11} and S_{22} vary slightly (if compared at each frequency), the tendencies that they exhibit for variable ground plane length is identical. Therefore, in the following discussion, only $|S_{11}|$ and $|S_{21}|$ are considered. One of the design goals is to achieve reflection coefficients
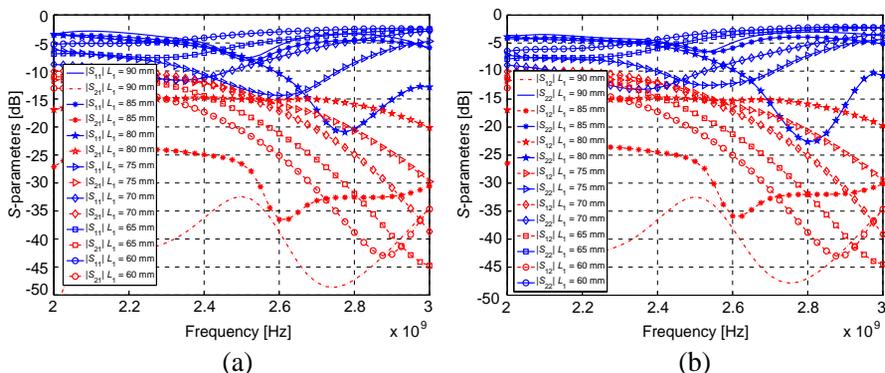
Figure 2. Simulated S-parameters of HEMA for variable ground plane lengths, L_1. (a) Simulated $|S_{11}|$ and $|S_{21}|$. (b) Simulated $|S_{22}|$ and $|S_{12}|$.

($|S_{11}|$ and $|S_{22}|$) lower than $-10\,\mathrm{dB}$ centered around $2.45\,\mathrm{GHz}$ (f_c), the region that is considered the impedance bandwidth of the antenna. Additionally, signal coupling from one port to the other, which is given by $|S_{21}|$ and $|S_{12}|$, is desired to be lower than $-20\,\mathrm{dB}$ to achieve lower signal correlation between antennas.

When $L_1 = 80\,\mathrm{mm}$, an impedance bandwidth of $400\,\mathrm{MHz}$ centered around $2.8\,\mathrm{GHz}$ can be achieved, which is unfortunately not at the desired center frequency. It is evident that this center frequency corresponding to the lowest $|S_{11}|$ value shifts towards lower frequencies when L_1 is decreased. When L_1 is smaller than $70\,\mathrm{mm}$, the reflection coefficients become undesirably high ($> -10\,\mathrm{dB}$). Furthermore, when the $-10\,\mathrm{dB}$ impedance bandwidth is considered, the signal coupled from Port 2 to 1 ($|S_{21}|$) is greater than $-15\,\mathrm{dB}$ for all values of L_1. The impedance bandwidths that can be achieved for $L_1 = 75\,\mathrm{mm}$ and $70\,\mathrm{mm}$ are $375\,\mathrm{MHz}$ and $300\,\mathrm{MHz}$, respectively. Since for $L_1 = 70\,\mathrm{mm}$, $|S_{11}|$ is centered closer to f_c than that for $L_1 = 75\,\mathrm{mm}$, $L_1 = 70$ is used in the subsequent design process.

By varying the ground plane length, it is possible to adjust reflection coefficients to the desired center frequency and achieve adequate impedance bandwidth, as shown earlier (see Figure 2). But further improvements are necessary to lower the undesired higher signal coupling ($> -15\,\mathrm{dB}$). The basic idea behind reducing the signal coupling between ports is to reduce the current flow between them by introducing a slit in the ground plane. First, a rectangular slit ($W_1 = W_2$) is introduced (see Figure 1(b)). S-parameters are simulated by varying the width of the slit W_1 from $1\,\mathrm{mm}$ to $6\,\mathrm{mm}$, and

the results are shown in Figure 3. The length of the slit is 25 mm, which is kept constant. It is evident that the frequency where the minimum $|S_{11}|$ occurs shifts to higher frequencies with the increase of slit width. The impedance bandwidth varies slightly for different slit widths. The minimum and maximum values, 210 MHz and 267 MHz, are achieved when $W_1 = 5$ mm and $W_1 = 4$ mm, respectively. The effect of slit width on $|S_{12}|$ and $|S_{21}|$ is very evident. The maximum value of $|S_{21}|$ decreases from -14 dB to -23 dB with the increase in slit width. As expected, the wider the slit width, the lower the signal coupling between the ports.
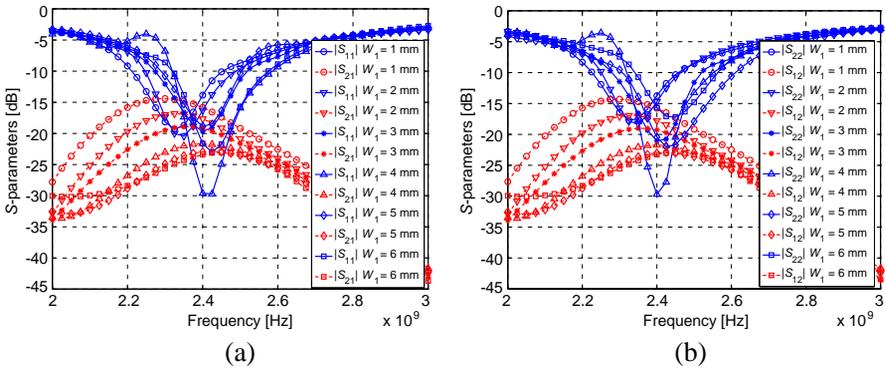
Figure 3. Simulated S-parameters of HEMA for variable slit widths W_1. Ground plane length $L_1 = 70$ mm. (a) Simulated $|S_{11}|$ and $|S_{21}|$. (b) Simulated $|S_{22}|$ and $|S_{12}|$.

By considering the impedance bandwidth and signal coupling, a slit width of 4 mm and a ground plane length of 70 mm seem to be a good choice for the antenna design. Even though the previously mentioned impedance bandwidth is about 267 MHz for this case, when both $|S_{11}|$ and $|S_{22}|$ are considered, this is reduced to 230 MHz since they are not perfectly aligned (compare Figures 3(a) and 3(b)). The antenna achieves lower signal coupling over the entire frequency range, which is less than -21.6 dB. When the lowest values of $|S_{11}|$ and $|S_{22}|$ are considered, they are not yet centered at f_c.

Further improvement in the antenna design is investigated by changing the shape of the slit in the ground plane. As a simple modification to the rectangular slit, a Y-shaped slit is introduced (see Figure 1(b)). Figure 4 shows the simulated S-parameters of the antenna for variable W_2 values. W_2 is varied from 5 mm to 10 mm in 1 mm increments W_1 is kept at 4 mm. The lowest values of $|S_{11}|$ and $|S_{22}|$ shift to higher frequencies with increasing W_2 values.
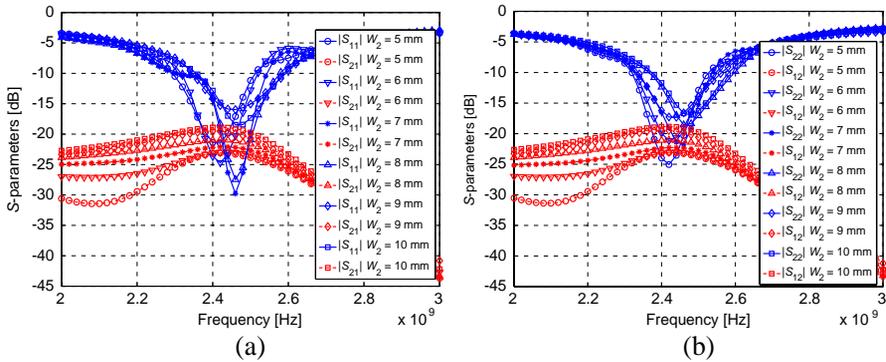
Figure 4. Simulated S-parameters of HEMA for variable W_2 values. Ground plane length $L_1 = 70\,\text{mm}$ and $W_1 = 4\,\text{mm}$. (a) Simulated $|S_{11}|$ and $|S_{21}|$. (b) Simulated $|S_{22}|$ and $|S_{12}|$.

Furthermore, $|S_{21}|$ and $|S_{12}|$ values for all W_2 values are lower than $-18.8\,\text{dB}$ over the entire simulation frequency range. This number is $-14.3\,\text{dB}$ for the rectangular slit (see Figure 3). When only $|S_{11}|$ is considered, the highest $-10\,\text{dB}$ impedance bandwidth is achieved for $W_2 = 8\,\text{mm}$, which is 260\,MHz. The lowest value of this is achieved when $W_2 = 6\,\text{mm}$, which is 200\,MHz. For both values of $W_2 = 7\,\text{mm}$ and $W_2 = 8\,\text{mm}$, $|S_{11}|$ is centered around 2.45\,GHz, which is one of the design goals. But the impedance bandwidth is 15\,MHz lower for the $W_2 = 7\,\text{mm}$ case than that of the latter case. When both $|S_{11}|$ and $|S_{22}|$ are considered, an impedance bandwidth of 235\,MHz is achievable for $W_2 = 8\,\text{mm}$. $|S_{21}|$ and $|S_{12}|$ values are lower than $-21\,\text{dB}$ over the entire simulated frequency range.

2.2. Substrate Material

The effective wavelength, λ_{eff} of an electromagnetic wave at a given frequency f_c, is inversely proportional to the square root of the product of permittivity and permeability of the medium, i.e., $\lambda_{eff} = \frac{1}{f_c\sqrt{\epsilon\mu}}$, where $\epsilon = \epsilon_r\epsilon_0$, and $\mu = \mu_r\mu_0$. The permittivity and the permeability in a vacuum are denoted by ϵ_0 and μ_0, respectively. The relative permittivity and permeability are denoted by ϵ_r and μ_r, respectively. Use of a ferrite substrate instead of a dielectric substrate for an antenna causes a lower λ_{eff}, thus resulting in a smaller dimension of the antenna structure. The reason for using ferrite material just below each meander structure is the higher loss of the used ferrite material. If ferrite material is used as substrate material instead of

the FR4 substrate, then the design would suffer from lower radiation efficiency. In this case, simulations show that the antenna efficiency would be 27%. Therefore, for HEMA, ferrite material is only used beneath each meander structure. The Y-shaped slit on the ground plane is used to reduce the signal coupling between the ports, i.e., to reduce forward and reverse transmission coefficients ($|S_{21}|$, and $|S_{12}|$). Among other parameters, low dielectric losses in substrate material, low reflection coefficients, and low transmission coefficients enhance antenna efficiency.

2.3. Fabricated Antenna

According to the simulation results obtained in Section 2.1, an antenna is fabricated. Figure 5 shows the fabricated antenna. The antenna model consists of two spatially separated half-cycle microstrip meander structures: a ferrite substrate below each meander structure, and an FR4 substrate covered by the ground. A commercially available FR4 PCB is used as the system board. The dimensions of the meander structure are shown in Figure 5(a). A ferrite substrate of dimensions $8 \times 6 \times 1.5\,\text{mm}^3$ has a permittivity of 6.6 and a permeability of 1.8, with corresponding loss tangents of 0.014 and 0.112, respectively. Permittivity and loss tangent values of an FR4 substrate ($90 \times 60 \times 1\,\text{mm}^3$) are 4.4 and 0.02, respectively. The size of the ground plane is $70 \times 60\,\text{mm}^2$ and has a Y-shaped slit, where $W_1 = 4\,\text{mm}$, and $W_2 = 8\,\text{mm}$ (see Figure 5(b)).

                    (a)   (b)
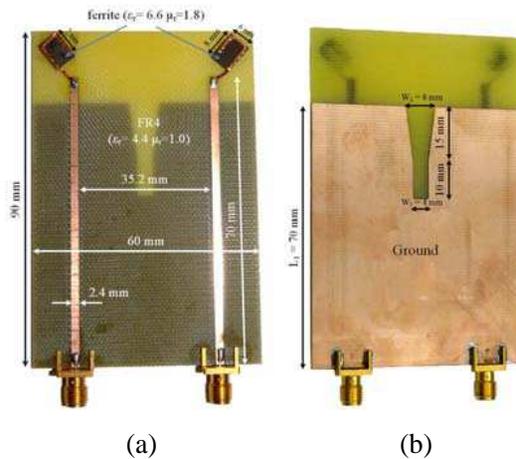
Figure 5. Top and bottom views of fabricated HEMA. (a) Top view. (b) Bottom view.

3. SYSTEM MODEL AND PERFORMANCE EVALUATION

3.1. MIMO Channel Model

The received signal of a MIMO system with N_T transmit antennas and N_R receive antennas can be written as [1]

$$\mathbf{y} = \sqrt{\frac{\rho}{N_T}}\mathbf{Hx} + \mathbf{n} \tag{1}$$

where ρ/N_T denotes the SNR at each receiver antenna element, $\mathbf{y}$ is the $(N_R \times 1)$ complex received signal vector, $\mathbf{x}$ is the $(N_T \times 1)$ complex normalized transmit signal vector, $\mathbf{H}$ is the complex $(N_R \times N_T)$ MIMO channel matrix, and $\mathbf{n}$ is the $(N_R \times 1)$ complex zero-mean additive white Gaussian noise vector with covariance matrix $E\{\mathbf{nn}^*\} = \mathbf{I}_{N_R}$.

The MIMO channel matrix $\mathbf{H}$ for a correlated channel can be separated into a constant matrix $\mathbf{H}_{los}$, which represents the line of sight (LOS), and a variable matrix $\mathbf{H}_{nlos}$, as follows [28]:

$$\mathbf{H} = \sqrt{\frac{K}{K+1}}\mathbf{H}_{los} + \sqrt{\frac{1}{K+1}}\mathbf{H}_{nlos} \tag{2}$$

where K is the Ricean K-factor, the elements of $\mathbf{H}_{nlos}$ are correlated zero-mean unit variance complex Gaussian variables, the elements of the fixed line-of-sight matrix $\mathbf{H}_{los}$ are written as $\exp(j\phi_{i,j})$, and i and j are the TX and RX antenna index, respectively. The notation $\exp(j\phi_{i,j})$ is the phase difference between the ith transmit and jth receive antenna [29]. The non-line-of-sight channel matrix is defined as [28]

$$\mathbf{H}_{nlos} = \mathbf{R}_R^{1/2}\mathbf{H}_{iid}\mathbf{R}_T^{1/2} \tag{3}$$

where, $\mathbf{R}_R$ and $\mathbf{R}_T$ denote the RX and TX spatial correlation matrices, respectively, and $\mathbf{H}_{iid} \in C^{N_R \times N_T}$ is a matrix of identical and independent (iid) complex Gaussian fading coefficients. In this paper, the line-of-sight component is not considered in the simulations, because most channels are under a multipath rich environment.

3.2. Spatial Correlation of Radiation Patterns

A closed-form formula for the spacial correlation coefficient of a 3-D multiple antenna array with arbitrary array configuration was presented in [30]. Since the structure of the antenna presented in this paper is planar, and non-uniform angular energy distribution is assumed, the formula presented in [30] is not used.

The correlation coefficient of the l-th TX antenna and the m-th RX antenna can be expressed using the angular distribution of the received power, i.e., the power angular spectrum (PAS) $S(\Omega)$ and far-field electric field $\underline{E}$ by [9] as

$$r_{l,m} = \frac{\int_\Omega S(\Omega)\underline{E}_l(\Omega)\underline{E}_m^*(\Omega)d\Omega}{\int_\Omega S(\Omega)|\underline{E}_{iso}(\Omega)|^2 d\Omega} \tag{4}$$

where $\underline{E}_{iso}(\Omega)$ is the far field of ideal isotropic radiators, and $l, m \in \{1, 2\}$ denotes TX and RX antenna indices. In (4), normalization is done with respect to the antenna gain of the ideal isotropic radiator. Normalization in the conventional definition of correlation coefficients does not take into account non-uniformly distributed $S(\Omega)$ or non-uniform antenna gain. Since the spatial correlation is normalized with respect to the gain of the ideal isotropic radiator, the envelope of (4) is not necessarily lower than one [9]. Assuming that the power angular spectrum over the azimuth angle and the elevation angle are independent, $S(\Omega)$ can be expressed as a product of power angular spectrums over the azimuth angle $S_\phi(\phi)$ and elevation angle $S_\theta(\theta)$, respectively [31]. Furthermore, assuming that the elevation angle spread is smaller than the azimuth angle spread and that received signals are concentrated over the azimuth plane, $S_\theta(\theta)$ can be expressed in the form of the delta function, $\delta(\theta - \pi/2)$ [8]. It has been shown that a Laplacian distribution offers the best fit for the power angular spectrum, for both urban and rural areas [28], which can be expressed as

$$S_\phi(\phi) = c \cdot e^{-\frac{\sqrt{2}}{\sigma_\phi}|\phi - \phi_c|}, \quad \phi, \phi_c \in [-\pi, \pi) \tag{5}$$

where ϕ is the azimuth angle, ϕ_c the mean angle of arrival (AoA) of the cluster, and σ_ϕ the standard deviation of the power azimuth spectrum that controls the angular spread. The constant c is determined as $(\sqrt{2}\sigma_\phi(1 - e^{-\sqrt{2}\pi/\sigma_\phi}))^{-1}$ by using the integration property of a probability density function, i.e., $\int_{-\infty}^{\infty} S_\phi(\phi)d\phi = 1$. Correlation coefficients are computed according to (4) by using the far-field electric field components obtained by FEKO simulations for performance evaluation of the system.

3.3. Mutual Impedance

The spatial channel matrix in (3), taking mutual coupling and correlation into consideration at both transmitter and receiver ends, is expanded [32] as

$$\mathbf{H} = \mathbf{M}_R(\eta_R\mathbf{R}_R)^{\frac{1}{2}}\mathbf{H}_{iid}(\eta_T\mathbf{R}_T)^{\frac{1}{2}}\mathbf{M}_T \tag{6}$$

where η_R and η_T are the receiver and transmitter efficiencies, respectively, and $\mathbf{M}_R$, $\mathbf{R}_R$, $\mathbf{M}_T$, and $\mathbf{R}_T$ denote the mutual coupling and correlation matrices at the receiver and transmitter, respectively. The transmitter and receiver coupling matrices are given by

$$\mathbf{M} = 2Z_0\mathbf{Y} \tag{7}$$

where

$$\mathbf{Y} = [\dot{\mathbf{Z}}_M + \mathbf{Z}]^{-1} \tag{8}$$

is the array admittance matrix [32] (here, subscripts R and T were omitted for simplicity), Z_0 the characteristic impedance of the transmission line connected to each antenna, $\dot{\mathbf{Z}}_M$ the matching impedance of each antenna, and $\mathbf{Z}$ the mutual impedance matrix.

The mutual impedance matrix $\mathbf{Z}$ can be computed in terms of the scattering matrix $\mathbf{S}$ [33] as

$$\mathbf{Z} = [\mathbf{I} + \mathbf{S}][\mathbf{I} - \mathbf{S}]^{-1} \tag{9}$$

where $\mathbf{I}$ is the identity matrix.

For performance evaluation, as will be described in the next subsection, a more realistic channel matrix is computed according to (6), whereas $\mathbf{H}$ in (3) has been used in most literature, e.g., [8, 9], for simplicity. In this paper, the impedance of matching networks, $\dot{\mathbf{Z}}_M$, is not considered in the calculation of admittance matrices, $\mathbf{Y}$, and mutual impedance matrices, $\mathbf{Z}$, are calculated by using the scattering matrices, $\mathbf{S}$, obtained by FEKO simulations.

3.4. Performance Evaluation

Generally, performance of a communication system is evaluated by capacity or BER. Capacity provides information on how many bits can be transmitted per unit time and per unit bandwidth with zero bit errors, and BER provides information on how many bits will be erroneous on average at a SNR. The channel matrix in (2) is required to calculate both performances. In this paper, the line-of-sight component is not considered. This assumption is valid for a typical multipath rich environment. Hence, only the ideal NLOS channel matrix in (3) or its extended channel matrix in (6) are used for performance evaluation.

For BER evaluation, Alamouti's diversity scheme presented in [34] was used in [9] and also in this paper for comparison. This simple diversity scheme improves the signal quality at the receiver and achieves a diversity order of $2M$, where M is the number of receive antennas, and two antennas are used at the transmitter end. This scheme assumes perfect channel information at the receiver end for

signal detection and no channel information at the transmitter end. Sensitivity to fading is decreased, which allows for usage of higher-order modulation techniques to increase the data rate. For simplicity, in this paper, the binary phase shift keying (BPSK) modulation is used, and the BER is calculated and compared with that of a two TX- and two RX-antenna system.

The ergodic channel capacity of a MIMO system with N_T transmit antennas and N_R receive antennas without channel information available at the transmitter end is [2]

$$C = E\left[\log_2 \det\left[\mathbf{I}_{N_R} + \frac{\rho}{N_T}\mathbf{H}\mathbf{H}^*\right]\right] \quad \left[\frac{\text{bits}}{\text{s} \cdot \text{Hz}}\right] \qquad (10)$$

where $E[\text{X}]$ is the expectation of a random variable X.

In the derivation of (10), the N_T components of the transmitted signal are assumed to be statistically independent, of equal power, and normally distributed. This capacity is computed using random channel matrix realizations, $\mathbf{H}$, for comparison with those of the proposed antenna. This choice is made because of the simple transmission scheme also used in this paper for evaluating BER performance, which does not require channel matrix information at the transmitter end.

4. MEASUREMENT RESULTS OF FABRICATED HEMA

Figure 5 shows the fabricated HEMA. The simulated and measured S-parameters of the HEMA are compared in Figure 6. Simulated as well as measured forward- and reverse-voltage gains, S_{21} and S_{12}, are less than $-21\,\text{dB}$ in the simulated/measured frequency band, $2\,\text{GHz}$ to $3\,\text{GHz}$. These low values of $|S_{21}|$ and $|S_{12}|$ assure a
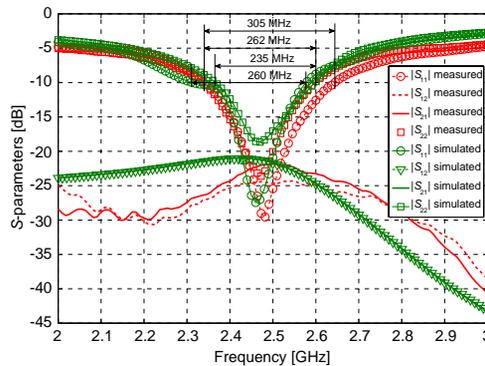
Figure 6. Simulated and measured S-parameters of HEMA.

very low signal coupling between the two antennas (ports), which is required. The impedance bandwidth of each port, which is measured at $|S_{ii}| = -10$ dB, where $i \in \{1, 2\}$, is as follows: Port 1 has simulated and measured impedance bandwidths of 262 MHz and 305 MHz, respectively, whereas these values for port 2 are 262 MHz and 235 MHz, respectively. When the reflection coefficients of both antennas ($|S_{11}|$ and $|S_{22}|$) are considered together, the fabricated antenna has an impedance bandwidth of 262 MHz. The measured and simulated reflection coefficients of port 2 ($|S_{22}|$) are almost aligned but have a 5 dB difference at the center frequency, whereas this is only 2 dB for port 1 ($|S_{11}|$), but the curves are shifted approximately 20 MHz at their minimum values. In general, the simulated S-parameter values agree with that of the fabricated antenna. S-parameters of the fabricated HEMA were measured by using an Anritsu MS2026A VNA Master network analyzer.

Simulated three-dimensional gain patterns of the HEMA are shown in Figure 7. Figures 7(a) and 7(b) show the gain patterns when each port was individually excited, i.e, only port 1 was excited for the case shown in Figure 7(a), and only port 2 was excited for the case shown in Figure 7(b). The maximum gain of each antenna is 2.2 dB and 2.3 dB, respectively. In the proceeding performance evaluations, the radiation patterns for elevation angle $\theta = 90°$ and azimuth angle $\phi = -180° \ldots 180°$ were used, because a mobile handset is typically held in an upright position, and most of the electromagnetic field reaching a mobile device is assumed to be azimuthal. The 2D radiation patterns were measured in an anechoic chamber by using the HEMA and a horn antenna as the transmitter and the receiver, respectively.

(a)   (b)
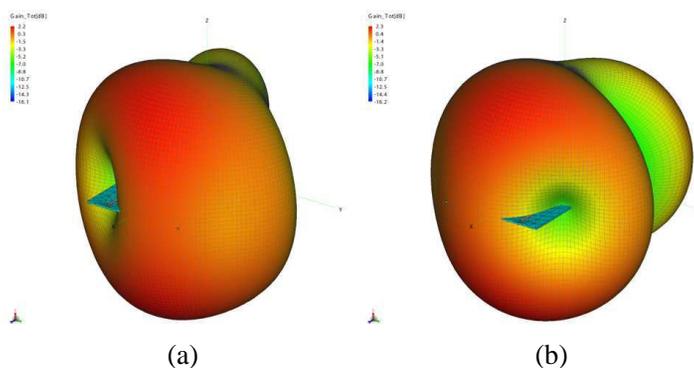
Figure 7. Simulated radiation patterns of HEMA. (a) Only port 1 excited. (b) Only port 2 excited.

An Agilent E4416A power meter was used to measure the received power. When port 1 was fed by a continuous sinusoidal signal at 2.45 GHz, a 50 Ω load was connected at port 2, and vice versa. The antenna was mounted on a Micos DT-80 rotation stage and rotated in 2° increments, and the received power was registered. Simulated and measured radiation patterns of the HEMA were normalized and shown in Figure 8. The 2D patterns were normalized in order to be easily compared. The gain values vary between the maximum and minimum of about 3 dB and 7 dB for simulated and measured patterns, respectively, when the azimuth angle varies from −180° to 180°. The greater variations in measured pattern could be caused by measurement errors and also from the dependency of gain for various ϕ angles, as shown in Figure 9. The difference between the highest and lowest gain values for $\phi = 86°$, $\phi = 88°$, $\phi = 90°$, $\phi = 92°$, and $\phi = 94°$ are 5.36 dB, 4.09 dB, 3.06 dB, 2.54 dB, and 3.09 dB, respectively. So slight variations in antenna orientation will affect the variations in gain.
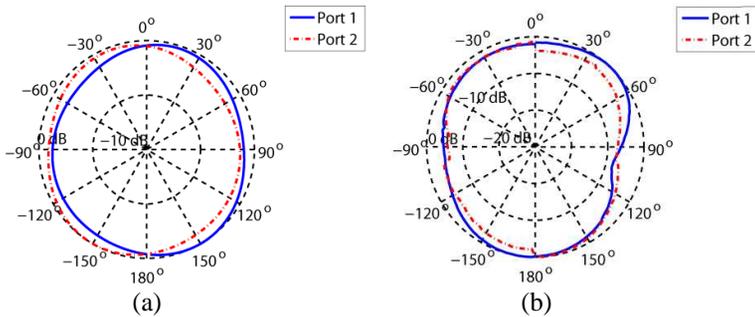
Figure 8. Simulated and measured radiation patterns of HEMA. Both patterns are shown for $\phi = 90°$ and $\theta = −180° \ldots + 180°$. (a) Total gain. (b) Normalized total measured power.
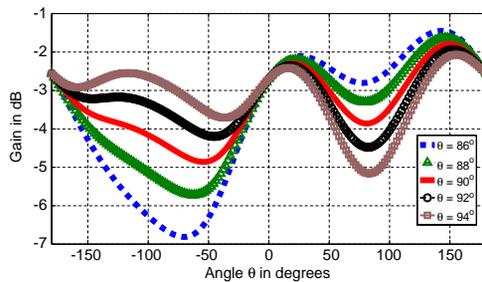
Figure 9. Simulated gain of HEMA vs. azimuth angle with elevation angle, θ, as a parameter.

5. PERFORMANCE ANALYSIS

A microwave parametric evaluation of the antennas was done in Section 4. In this section, the antenna is evaluated by using communication system performance metrics such as BER and channel capacity. In order to evaluate these performance metrics, the channel matrix has to be realized according to (6), which includes the effects of mutual coupling between antennas, radiation efficiency of the antennas, and correlation between the transmitter-side and receiver-side radiation patterns. Simulated S-parameters at the center frequency, f_c, were used to calculate the mutual impedance matrices M_R and M_T, from (7)–(9). Since no impedance matching network was used, $\dot{\mathbf{Z}}_M$ was assumed to be the identity matrix. By using the simulated 2D radiation patterns (see Figure 8(a)), correlation coefficients were calculated according to (4) and are shown in Figure 10. The reason for using the simulated 2D radiation patterns for calculating correlation coefficients is that the electric field strengths are required according to (4), and those cannot be measured but can be obtained by simulations. These correlation values are used to generate $\mathbf{R}_T$ and $\mathbf{R}_R$ matrices in (6) for each angle. According to the conventional definition of correlation, the envelope is always lower than one. Since (4) is normalized with respect to the antenna gain of ideal isotropic radiation, it can be larger than one, as observed in Figure 10 [9].

The 2×2 MIMO transmission scheme introduced in [34] was used for evaluating BER performance. Bit error rate was simulated for each angle and then averaged, as shown in Figure 11 (green curve). To
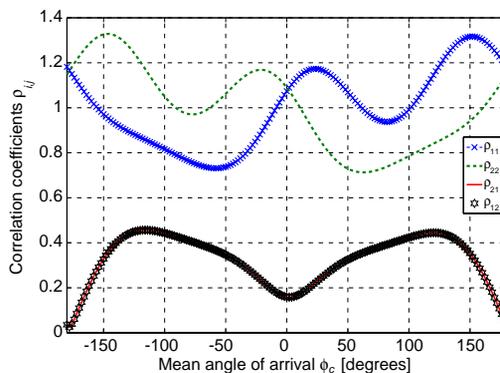
Figure 10. Simulated correlation coefficients of HEMA vs. mean angle of arrival ϕ_c.
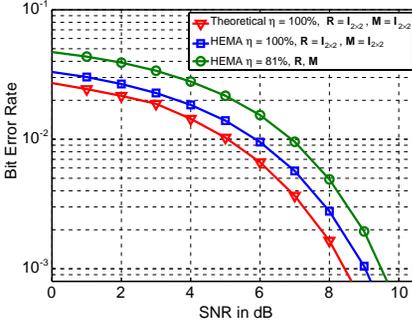
Figure 11. Average BER comparison of HEMA, and theoretical 2×2 MIMO vs. SNR using Alamouti scheme under Rayleigh fading channel.
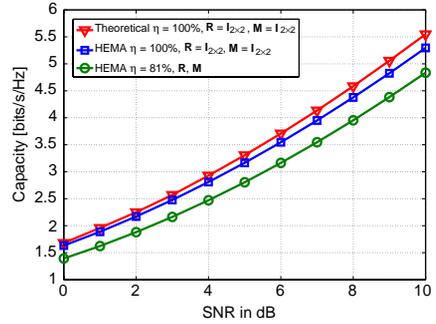
Figure 12. Average ergodic capacity comparison of HEMA, and theoretical 2×2 MIMO vs. SNR.

see the effect of antenna efficiency and correlation between radiation patterns on system performance, two more curves are presented. The scheme presented in [34] does not take antenna efficiency, mutual coupling, and correlation into account when generating the channel matrix, $\mathbf{H}$, i.e., it is assumed that $\mathbf{M}_T = \mathbf{M}_R = \mathbf{R}_T = \mathbf{R}_R = \mathbf{I}_2$ and $\eta_R = \eta_T = 100\%$ (see red curve) and hence is used as the reference. The radiation efficiency of the HEMA obtained by simulations is 81%. At the BER of 10^{-3}, the HEMA needs a 1.1 dB signal-to-noise ratio increment with respect to the reference curve to achieve the same performance. To see the effect of radiation efficiency on bit error rate, BER is simulated for the ideal antenna efficiency, $\eta = 100\%$ (blue curve). The correlation and mutual impedance matrices used are the same as for the green curve. When radiation efficiency is increased to 100%, a BER of 10^{-3} is achieved for 0.53 dB less SNR, compared to when the efficiency is 81% (compare blue and green curves). When compared with the ideal curve (red curve), it can be seen that the non-ideal correlation and mutual impedance matrices cause degradation in system performance, even though the antenna has maximum efficiency. The performance degradation in this case is about 0.6 dB (compare blue and red curves).

Simulated ergodic capacity of the system is shown in Figure 12. Capacity is calculated according to (10) for three different cases and is color-coded the same as for BER. For example, to achieve a capacity of 3 bits/s/Hz, the HEMA requires 1.4 dB higher SNR than for the ideal case (compare red and green curves). In evaluating ergodic capacity,

by keeping the correlation matrix and the mutual impedance matrix of the HEMA unchanged and only increasing the efficiency to 100%, the blue curve is generated. Now it needs only 0.4 dB higher SNR than for the ideal case to achieve the capacity of 3 bits/s/Hz. As shown, the antenna efficiency has a greater impact on the performance of the system than the correlation matrix and the mutual impedance matrix.

Table 1 compares bandwidth, antenna efficiency, PCB size, antenna element size, and envelope correlation coefficient of the proposed antenna with that presented in [18–22]. The envelope correlation coefficient of the proposed antenna calculated according to Eq. (11) in [27] is shown in Figure 13. It is only used for comparison purposes, since all other antennas listed in the table have presented the correlation coefficients calculated using the same formula. The impedance bandwidth is given for a specific VSWR or reflection coefficient value $|S_{ii}|$, where i is the port index. A VSWR of 3 : 1, 2.5 : 1, and 2 : 1 corresponds to a reflection coefficient of -6 dB, -7.4 dB, and -9.6 dB, respectively. For each of the preceding cases, the percentage of reflected power is 25.0%, 18.4%, and 11.0%, respectively. The lower the percentage, the more the power is transferred to the device. For the previously discussed VSWRs, the bandwidth of the proposed antenna is 519 MHz, 391 MHz, and 262 MHz, respectively. When compared with the listed antennas in Table 1, the proposed antenna has a lower bandwidth than only the one presented in [21]. But it has a lower efficiency and higher correlation coefficient, which are more critical factors when other performance matrices (BER and capacity) are considered. Lower correlation and higher efficiency improve the BER and capacity. Even though the area of PCB of the antenna presented in [21] is 17% smaller, its element size (area) is 3.9 times (296%) greater, and the correlation coefficient is more
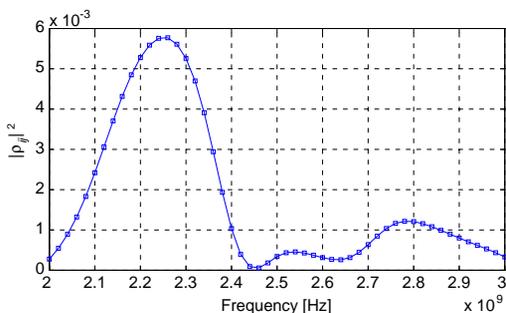
Figure 13. Envelope correlation of HEMA calculated according to Eq. (11) in [27].

than eight times greater than that of the proposed antenna. The antenna presented in [19] has the highest efficiency of all listed. But its bandwidth is much less than the proposed antenna (200 MHZ compared to 519 MHz). Its PCB size is 11% larger and the element size is 11.25 times larger than the proposed antenna. The antenna presented in [19] has the smallest PCB size $(10 \times 20\,\text{mm}^2)$, which is 27 times smaller than the proposed antenna. But its correlation coefficients are more than 250 times greater, and the bandwidth is 111 MHz (28%) lower than the proposed antenna.

6. CONCLUSION

A high-efficiency half-cycle microstrip meander antenna with partial ferrite substrate was fabricated and tested. S-parameters and radiation patterns were measured in the lab and compared with those from simulations. An impedance bandwidth of 262 MHz was achieved by the fabricated HEMA. Simulations showed that the HEMA has a high antenna efficiency of 81%. Using the simulated far-field radiation patterns and S-parameters, ergodic capacity and BER performance of HEMA were evaluated. The effect of antenna efficiency, non-ideal correlation, and mutual impedance matrices on BER and ergodic capacity was evident. The most critical parameter out of these three is antenna efficiency. When compared to the ideal case ($\mathbf{M}_T = \mathbf{M}_R = \mathbf{R}_T = \mathbf{R}_R = \mathbf{I}_2$ and $\eta_R = \eta_T = 100\%$), the HEMA shows only 1.0 dB degradation in SNR for a BER of 10^{-3}, and 1.4 dB degradation in SNR for 3 bits/s/Hz capacity. In other words, to achieve a BER of 10^{-3}, the HEMA requires a 1.0 dB higher SNR than that for the ideal case. And it requires a 1.4 dB higher SNR to achieve the same capacity of 3 bits/s/Hz than that for the ideal case. If the HEMA had an efficiency of 100%, then these values would be 0.6 dB and 0.3 dB, respectively. It is evident that the lower the antenna efficiency, the lower the performance.

The overall dimensions of the antenna are intentionally designed to be comparable to that of current cellular phones, and the wide frequency bandwidth allows it to be used in 3GPP LTE mobile standards.

ACKNOWLEDGMENT

REFERENCES

1. Telatar, E., "Capacity of multiantenna Gaussian channels," *European Transactions on Telecommunications*, Vol. 10, 585–596, Nov.–Dec. 1999.

2. Foschini, G. S. and M. J. Gans, "On limits of wireless communications in a fading environment when using multiple antennas," *Wireless Personal Communications*, Vol. 6, 311–335, Mar. 1998.

3. Andrews, M. R., P. P. Mitra, and R. deCarvalho, "Trippling the capacity of wireless communications using electromagnetic polarization," *Nature*, Vol. 409, 316–318, Jan. 2001.

4. Dong, L., H. Ling, and R. W. Heath, Jr., "Multiple-input-multiple-output wireless communication systems using antenna patttern diversity," *IEEE Global Telecommunications Conference, GLOBECOMM' 2002*, 997–1001, Nov. 2002.

5. Vaughan, R. G. and J. B. Anderson, "A multiport patch antenna for mobile communications," *Proceedings of 14th European Microwave Conference*, 607–612, Oct. 1984.

6. Vaughan, R. G., "Two-port higher mode circular microstrip antennas," *IEEE Transactions on Antennas and Propagation*, Vol. 36, 309–321, Mar. 1988.

7. Dammerle, F. and W. Wiesbeck, "A biconical multibeam antenna for space-division multiple access," *IEEE Transactions on Antennas and Propagation*, Vol. 46, 782–787, Jun. 1998.

8. Forenza, A. and R. W. Heath, Jr., "Benefit of pattern diversity via two-element array of circular patch antennas in indoor clustered MIMO channels," *IEEE Transactions on Communications*, Vol. 54, 943–954, May 2006.

9. Forenza, A. and R. W. Heath, Jr., "Optimization methodology for designing 2-CPAs exploiting pattern diversity in clustered MIMO channels," *IEEE Transactions on Communications*, Vol. 56, 1748–1759, Oct. 2008.

10. Bae, S., Y.-K. Hong, J.-J. Lee, J.-H. Park, J. Jalli, G. Abo, H. M. Kwon, and C. K. K. Jayasooriya, "Miniature and higher-order mode ferrite MIMO ring patch antenna for mobile communication system," *Progress In Electromagnetics Research B*, Vol. 25, 53–74, 2010.

11. Piazza, D., P. Mookiah, M. D'Amico, and K. R. Dandekar, "Pattern reconfigurable circular patch antenna for MIMO communications," *Proceedings of RILEM Conference*, 2008.

12. Piazza, D., M. D'Amico, and K. R. Dandekar, "MIMO communi-

cation system with reconfigurable circular patch antennas," *IEEE Antennas and Propagation Society International Symposium (AP-SURSI)*, 1–4, Jul. 2008.

13. Jayasooriya, C., H. Kwon, S. Bae, and Y.-K. Hong, "Miniaturized multimode circular patch antennas for MIMO communications," *IEEE 70th Vehicular Technology Conference Fall (VTC 2009-Fall)*, 1–5, Sep. 20–23, 2009.

14. Jayasooriya, C. K., H. M. Kwon, S. Bae, and Y.-K. Hong, "Miniaturized circular antennas for MIMO communication systems — Pattern diversity," *2010 International ITG Workshop on Smart Antennas (WSA)*, 331–334, Feb. 23–24, 2010.

15. Jayasooriya, C. K. K., H. M. Kwon, S. Bae, and Y.-K. Hong, "Miniaturized single circular and single ring patch antenna for MIMO communications exploiting pattern diversity," *IEEE International Conference on Communications (ICC)*, 1–5, May 2010.

16. Rajo-Iglesias, E., O. Quevedo-Teruel, M. L. Pablo-Gonzalez, and M. Sanchez-Fernandez, "A compact dual mode microstrip patch antenna for MIMO applications," *Proceedings of IEEE Antennas and Propagation Society International Symposium*, 3651–3654, Jul. 2006.

17. Balanis, C. A., *Antenna Theory Analysis and Design,* 3rd Edition, John Wiley & Sons, Inc., New Jersey, 2005.

18. Yang, C., Y. Yao, and X. Chen, "Novel compact multiband MIMO antenna for mobile terminal," *International Journal of Antennas and Propagation*, Vol. 2012, 9, 2012.

19. Ssorin, V., A. Artemenko, A. Sevastyanov, and R. Maslennikov, "Compact bandwidth-optimized two element MIMO antenna system for 2.5–2.7 GHz band," *Proceedings of the 5th European Conference on Antennas and Propagation (EUCAP)*, 319–323, Apr. 2011.

20. Dioum, I., A. Diallo, C. Luxey, and S. Farsi, "Dual-band monopole MIMO antennas for LTE mobile phones," *ICECom, 2010 Conference Proceedings*, 1–4, Sep. 2010.

21. Li, W.-Y. and W.-J. Chen, "Concurrent 2-port/3-port MIMO antenna system for UMTS/LTE2500 operation in the mobile phone," *IEEE Antennas and Propagation Society International Symposium (APSURSI)*, 1918–1921. Jul. 2011.

22. Kuonanoja, R., "Low correlation handset antenna conguration for LTE MIMO applications," *IEEE Antennas and Propagation Society International Symposium (APSURSI)*, 1–4, Jul. 2010.

23. Lee, J., Y.-K. Hong, S. Bae, G. Abo, W.-M. Seong, and G.-H. Kim,

"Miniature long-term evolution (LTE) MIMO ferrite antenna," *IEEE Antennas and Wireless Propagation Letters*, Vol. 10, 603–606, 2011.

24. Bhatti, R., S. Yi, and S.-O. Park, "Compact antenna array with port decoupling for LTE-standardized mobile phones," *IEEE Antennas and Wireless Propagation Letters*, Vol. 8, 1430–1433, 2009.

25. Sato, H., T. Hayashi, Y. Koyanagi, and H. Morishita, "Small array antenna for 2×2 MIMO terminal using folded loop antenna," *First European Conference on Antennas and Propagation (EuCAP 2006)*, 1–5, Nov. 2006.

26. Sharawi, M., Y. Faouri, and S. Iqbal, "Design and fabrication of a dual electrically small MIMO antenna system for 4G terminals," *2011 German Microwave Conference (GeMIC)*, 1–4, Mar. 2011.

27. Blanch, S., J. Romeu, and I. Corbella, "Exact representation of antenna system diversity performance from input parameter description," *Electronics Letters*, Vol. 39, No. 9, 705–707, May 2003.

28. Pedersen, K. I., P. E. Mogensen, and B. H. Fleury, "Spatial channel characteristics in outdoor environments and their impact on BS antenna system performance," *Proceedings of 48th IEEE Vehicular Technology Conference*, 719–723, 1998.

29. Soma, P., D. Baum, V. Erceg, R. Krishnamoorthy, and A. Paulraj, "Analysis and modeling of multiple-input multiple output (MIMO) radio channel based on outdoor measurements conducted at 2.5 GHz for fixed BWA applications," *IEEE International Conference on Communications (ICC)*, Vol. 1, 272–276, 2002.

30. Lee, J.-H. and C.-C. Cheng, "Spatial correlation of multiple antenna arrays in wireless communication systems," *Progress In Electromagnetics Research*, Vol. 132, 347–368, 2012.

31. Correira, L. M., *Wireless Flexible Personalized Communications,* John Wiley & Sons, Inc., New York, 2001.

32. Alrabadi, O. N., C. B. Papadias, A. Kalis, N. Marchetti, and R. Rasad, "Spatial multiplexing via antenna switching," *IEEE Communication Letters*, Vol. 13, 594–596, 2009.

33. Pozar, D. M., *Microwave Engineering,* 3rd Edition, John Wiley & Sons, Inc., New Jersey, 2005.

34. Alamouti, S. M., "A simple transmit diversity technique for wireless communications," *IEEE Journal on Selected Areas in Communications*, Vol. 16, No. 8, 1451–1458, Oct. 1998.